## Analytical method

**Major and trace elements**. Major element contents were analyzed on fused glass disks using a Rigaku ZSX-100e X-ray fluorescence spectrometer and the analytical methods reported by Goto and Tatsumi (1996). Three repeated analyses of a basaltic reference material (BHVO-2) indicate the analytical precision was better than ±5% and the accuracy was better than ±2% for most major elements. Trace elements were analyzed with an iCAP-Q (Thermo Fisher) inductively coupled plasma mass spectrometer following the methods of Liu et al. (1996). Three repeated analyses of BHVO-2 indicate that the analytical precision for all the measured trace elements was better than 5%, and most trace element contents are consistent with their reference values to within ±5% (**Table A1**).

**Table A1** Trace element results (ppm) of the reference material BHVO-2.

| | BHVO-2-1 | BHVO-2-2 | BHVO-2-3 | Preferred value | 1RSD(%) | Accuracy |
|---|---|---|---|---|---|---|
| Sc | 31.38 | 31.78 | 32.22 | 33.00 | 1.3% | -3.7% |
| V | 299.6 | 305.3 | 309.9 | 308.0 | 1.7% | -1.0% |
| Cr | 287.0 | 269.2 | 284.2 | 293.0 | 3.4% | -4.4% |
| Co | 44.14 | 43.20 | 44.61 | 44.00 | 1.6% | 0.0% |
| Ni | 114.0 | 104.4 | 105.6 | 116.0 | 4.9% | -6.9% |
| Sr | 407.3 | 412.5 | 390.7 | 396.0 | 2.8% | 1.9% |
| Y | 24.38 | 25.22 | 25.23 | 26.00 | 1.9% | -4.1% |
| Zr | 157.0 | 156.5 | 162.1 | 170.0 | 2.0% | -6.7% |
| Nb | 17.97 | 16.77 | 17.83 | 18.30 | 3.7% | -4.2% |
| Ba | 129.8 | 132.2 | 128.7 | 131.0 | 1.4% | -0.6% |
| La | 15.71 | 15.36 | 15.22 | 15.20 | 1.6% | 1.5% |
| Ce | 36.66 | 35.68 | 36.96 | 37.60 | 1.8% | -3.1% |
| Pr | 4.80 | 4.82 | 4.93 | 5.35 | 1.4% | -9.3% |
| Nd | 24.39 | 23.42 | 23.14 | 24.50 | 2.8% | -3.5% |
| Sm | 5.81 | 5.72 | 5.94 | 6.10 | 1.8% | -4.5% |
| Eu | 2.07 | 2.07 | 2.00 | 2.07 | 2.0% | -1.2% |
| Gd | 5.51 | 5.74 | 5.53 | 6.16 | 2.2% | -9.2% |
| Tb | 0.91 | 0.86 | 0.89 | 0.92 | 2.8% | -3.4% |
| Dy | 5.28 | 4.90 | 4.88 | 5.28 | 4.5% | -4.9% |

| | | | | | | |
|---|---|---|---|---|---|---|
| Ho | 0.93 | 0.97 | 0.99 | 0.98 | 3.0% | -1.4% |
| Er | 2.33 | 2.53 | 2.39 | 2.56 | 4.3% | -5.6% |
| Tm | 0.32 | 0.30 | 0.30 | 0.34 | 4.8% | -9.5% |
| Yb | 1.86 | 1.89 | 1.90 | 2.01 | 1.0% | -6.3% |
| Lu | 0.26 | 0.28 | 0.27 | 0.28 | 2.3% | -3.6% |
| Hf | 4.08 | 4.11 | 4.22 | 4.32 | 1.8% | -4.2% |
| Ta | 1.05 | 1.14 | 1.06 | 1.15 | 4.5% | -5.7% |
| Th | 1.15 | 1.16 | 1.19 | 1.22 | 1.7% | -4.5% |
| U | 0.40 | 0.40 | 0.39 | 0.40 | 0.7% | -1.5% |

**Molybdenum isotopes**. The selected rocks and mineral separates were crushed in an agate mortar to ~200 mesh. Accurately weighed sample powders, which contain about 50–100 ng Mo, and appropriate amounts of a $^{97}$Mo–$^{100}$Mo double-spike (DS) solution were added to 50 mL PFA beakers. The contributions of sample and DS for Mo in the mixture was adjusted to around 1:1 (Zhang et al., 2018). The sample–spike mixtures were then digested in 12 ml of a 1:2 (by volume) mixture of concentrated $HNO_3$ (14 mol/L) and HF (22 mol/L) at 150˚C for 5 d. After digestion and drying at 120 ˚C, the samples were dissolved in 4 ml of concentrated HCl (12 mol/L), and then evaporated to dryness. The residue was re-dissolved in 6 ml of a mixture of HF (0.1 mol/L) and HCl (1 mol/L), at which point it was ready for column separation. The Mo purification was conducted with the BPHA resin (Li et al., 2014; Fan et al., 2020). The Mo solutions in 2% (v/v) $HNO_3$ were diluted to 150–200 ppb. Molybdenum isotopic measurements were conducted with a Neptune Plus (Thermo Fisher) multiple-collector inductively coupled plasma mass spectrometer. A quartz cyclonic spray chamber with a 50 μL/min PFA nebulizer were used for sample solution introduction. A high-performance jet sample cone and an X skimmer cone were used at the interface. At such conditions, the signal intensity of $^{95}$Mo is about 7-10 V for a one-ppm Mo solution and

all samples measured in this study have $^{95}$Mo signal > 0.5 volt. Each sample solution was measured for 40 cycles with an integration time of 4.194 s. After each sample analysis, the sample introduction system was subsequently washed with 2% $HNO_3$, mixture of 2% $HNO_3$ + 0.1% HF, and 2% $HNO_3$. Usually, the $^{100}$Mo signal decreased to < 1 mv after 3–5-minute wash. $^{99}$Ru was monitored for isobaric interference correction of $^{96}$Ru, $^{98}$Ru and $^{100}$Ru on Mo isotopes. However, all sample solutions measured in this study show extremely low Ru signal ($^{99}$Ru < 0.1 mV), which have negligible influence on Mo isotopes and thus no further correction of the interference of Ru was conducted during our experiment. The double spike data reduction was undertaken with an in-house Microsoft Virtual Basic program based on the mathematical algorithm of Zhang et al. (2015). Molybdenum isotopic compositions are reported as $\delta^{98/95}$Mo values relative to the pure Mo reference material NIST SRM 3134. The procedural blank during our study was 0.15 ± 0.08 ng (2SD; n = 3) of Mo, which is much lower than the total Mo in the analyzed samples (>100 ng). The external reproducibility of the NIST SRM 3134 standard solution was 0.06‰ (2SD; n = 18). Two rock reference materials (W-2a and BIR-1a) were analyzed along with our samples, which yielded $\delta^{98/95}$Mo = –0.12‰ ± 0.04‰ (2SE) and –0.20‰ ± 0.06‰ (2SE), respectively, which agree well with reported values for these standards (Fan et al., 2020; Zhao et al., 2016). The long-term reproducibility of the Mo isotopic measurements, based on two-year analyses of NIST SRM 3134 reference solutions and seawater samples, was ⩽ 0.07‰ (two standard deviations, 2s, n = 167) for $\delta^{98/95}$Mo. The Mo isotope analytical uncertainties of all samples measured in this study are reported in

2SE.

## Supporting figures

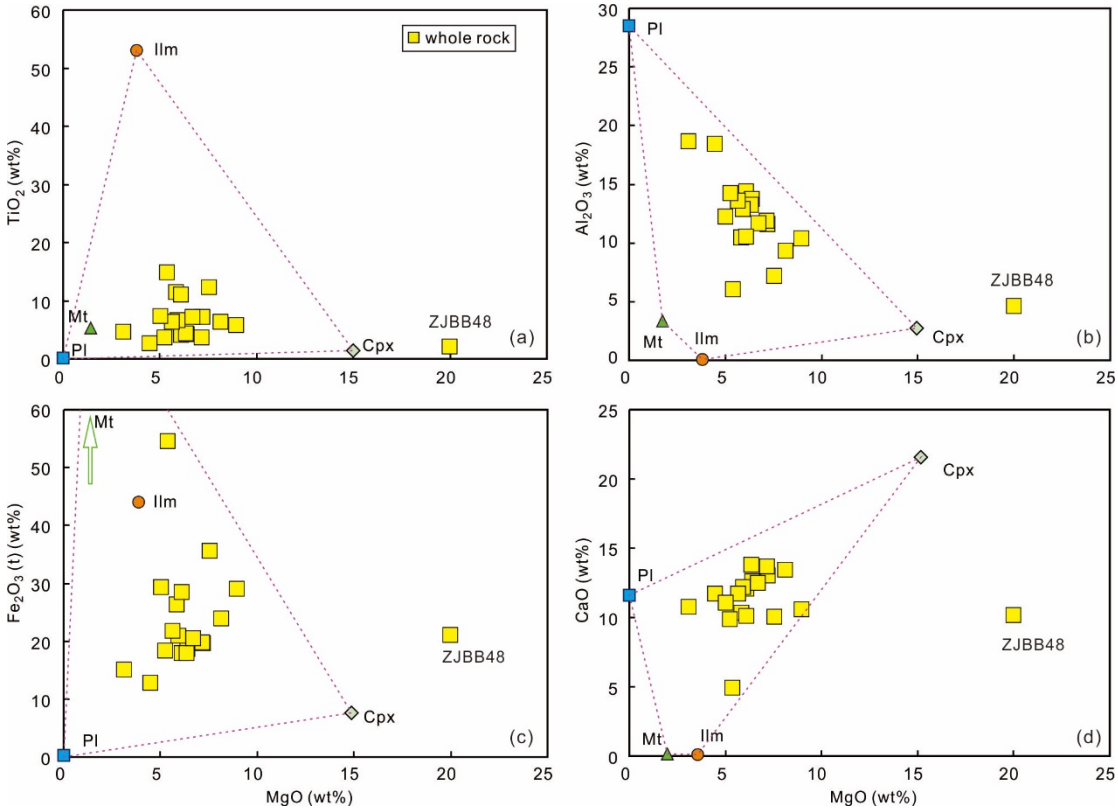


**Figure S1** Plots of (a) $TiO_2$, (b) $Al_2O_3$, (c) $Fe_2O_3$(t), and (d) CaO versus MgO. The mineral compositions are the average values for each mineral from previous studies. Mineral data sources: Cpx = Hou et al. (2012b) and Pang et al. (2009); Pl = Zhang et al. (2011); Mt = Liu et al. (2015); Ilm = Zheng et al. (2014). Mineral abbreviations: Cpx = clinopyroxene; Pl = plagioclase; Mt = magnetite; Ilm = ilmenite.

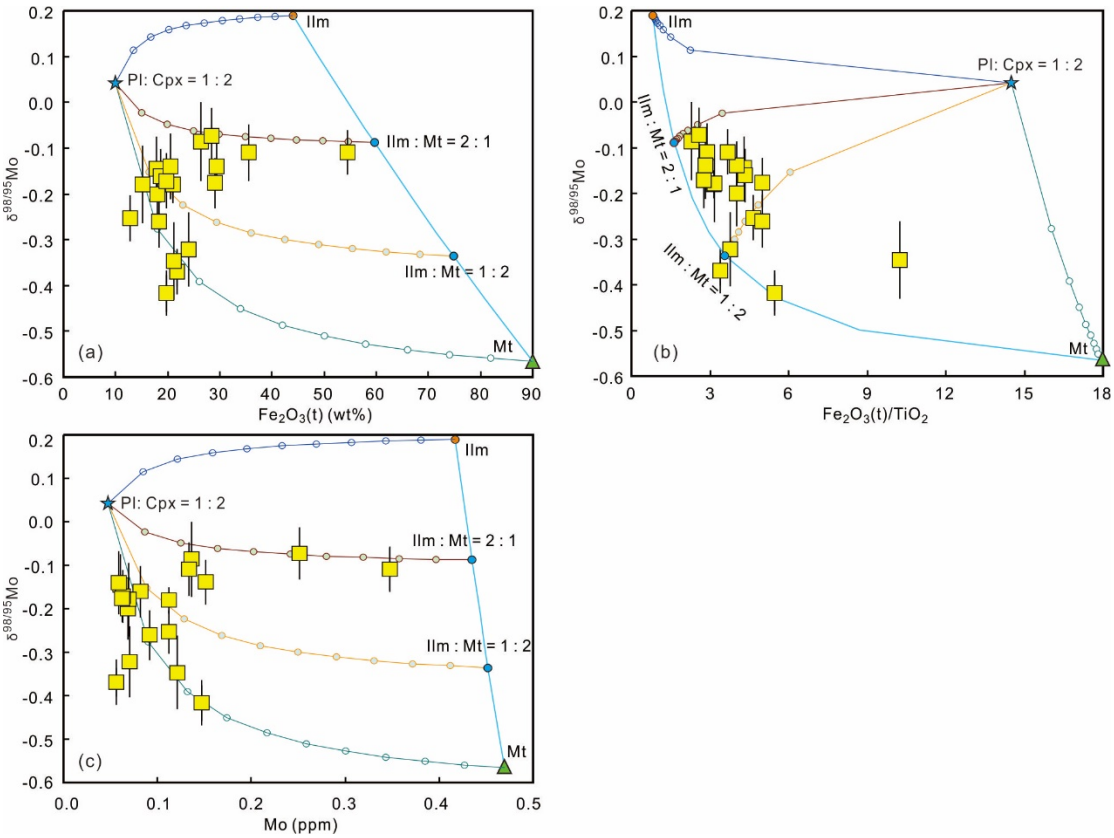


**Figure S2** Plots of $\delta^{98/95}$Mo versus (a) $Fe_2O_3(t)$, (b) $Fe_2O_3(t)/TiO_2$ and (c) Mo content. The lines between the minerals are the mass balance modeling trends. The blue stars represent a modeling end-member consisting of plagioclase and clinopyroxene with a ratio of 1:2. The mixing step is set to 10% between silicate end-member and Fe-Ti oxides. The error bars are in 2SE. The mass balance modeling parameters are listed in **Table S3**.

## References

Fan, J.-J., Li, J., Wang, Q., Zhang, L., Zhang, J., Zeng, X.-L., Ma, L., and Wang, Z.-L. (2020) High-precision molybdenum isotope analysis of low-Mo igneous rock samples by MC–ICP–MS. Chemical Geology, 545, 119648.

Goto, A., and Tatsumi, Y. (1996) Quantitative analyses of rock samples by an X-ray fluorescence spectrometer (II). The Rigaku Journal, 13(1), 20-39.

Hou, T., Zhang, Z., and Pirajno, F. (2012b) A new metallogenic model of the Panzhihua giant V–Ti–iron oxide deposit (Emeishan Large Igneous Province) based on high-Mg olivine-bearing wehrlite and new field evidence. International Geology Review, 54(15), 1721-1745.

Li, J., Liang, X.-R., Zhong, L.-F., Wang, X.-C., Ren, Z.-Y., Sun, S.-L., Zhang, Z.-F., and Xu, J.-F. (2014) Measurement of the Isotopic Composition of Molybdenum in Geological Samples by MC-ICP-MS using a Novel Chromatographic Extraction Technique. Geostandards and Geoanalytical

Research, 38(3), 345-354.

Liu, P.-P., Zhou, M.-F., Chen, W.T., Gao, J.-F., and Huang, X.-W. (2015) In-situ LA-ICP-MS trace elemental analyses of magnetite: Fe–Ti–(V) oxide-bearing mafic–ultramafic layered intrusions of the Emeishan Large Igneous Province, SW China. Ore Geology Reviews, 65, 853-871.

Liu, Y., Liu, H.C., and Li, X.H. (1996) Simultaneous and precise determination of 40 trace elements in rock samples using ICP-MS. Geochimica, 25(1), 552-558.

Pang, K.-N., Li, C., Zhou, M.-F., and Ripley, E.M. (2009) Mineral compositional constraints on petrogenesis and oxide ore genesis of the late Permian Panzhihua layered gabbroic intrusion, SW China. Lithos, 110(1), 199-214.

Zhang, L., Ren, Z.-Y., Xia, X.-P., Li, J., and Zhang, Z.-F. (2015) IsotopeMaker: A Matlab program for isotopic data reduction. International Journal of Mass Spectrometry, 392, 118-124.

Zhang, L., Li, J., Xu, Y.G., and Ren, Z.Y. (2018) The influence of the double spike proportion effect on stable isotope (Zn, Mo, Cd, and Sn) measurements by multicollector-inductively coupled plasma-mass spectrometry (MC-ICP-MS). Journal of Analytical Atomic Spectrometry, 33, 555-562.

Zhang, X., Zhang, J., Song, X., Deng, Y., Guan, J., and Zhang, W. (2011) Implications of compositions of plagioclase and olivine on the formation of the Panzhihua V-Ti magnetite deposit, Sichuan Province. Acta Petrologica Sinica, 27(12), 3675-3688.

Zheng, W., Deng, Y., Song, X., Chen, L., Yu, S., Zhou, G., Liu, S., and Xiang, J. (2014) Composition and genetic significance of the ilmenite of the Panzhihua intrusion. Acta Petrologica Sinica, 30(5), 1432-1442.

Zhao, P.-P., Li, J., Zhang, L., Wang, Z.-B., Kong, D.-X., Ma, J.-L., Wei, G.-J., and Xu, J.-F. (2016) Molybdenum Mass Fractions and Isotopic Compositions of International Geological Reference Materials. Geostandards and Geoanalytical Research, 40(2), 217-226.